PAN ARCHIVES OF ACOUSTICS
Vol. 43, No. 4, pp. 657–667 (2018)

DOI: 10.24425/aoa.2018.125159

Formation of Scattering Characteristics for Acoustical Ray Tracing Simulation

Srđan BOJIČIĆ, Dragana ŠUMARAC-PAVLOVIĆ, Miomir MIJIĆ

School of Electrical Engineering
University of Belgrade
Bulevar kralja Aleksandra 73, Belgrade, Serbia; e-mail: srdjan.bojicic@gmail.com, {dsumarac, emijic}@etf.rs

(*received September 26, 2017; accepted June 7, 2018*)

Ray tracing simulation of sound field in rooms is a common tool in room acoustic design for predicting impulse response. There are numerous commercial engineering tools utilising ray tracing simulation. A specific problem in the simulation is the modelling of diffuse reflections when contribution of individual surface is prevailing. The paper introduces modelling of scattering which is interesting when the whole impulse response of a room is not a goal but contribution of certain surface. The main goal of the project is to shape directivity characteristics of scattered reflection. Also, an innovative approach is suggested for converting the energy histogram information obtained by ray tracing into an "equivalent impulse response". The proposed algorithm is tested by comparing the results with measurements in a real sound field, realised in a scaled model where a diffusing surface is hardware-implemented.

Keywords: diffuse reflection; ray tracing; room acoustics; secondary source; scattering pattern.

1. Introduction

A beginning of the ray tracing in architectural acoustics dates from 1960's, when first publications appeared (Krokstad *et al.*, 1968). Nowadays, the hybrid approach in computer simulation of room acoustics is widely used, combining the ray tracing and image-source methods (Vorländer, 2013). Surfaces in a room are described by two numerical parameters: the absorption coefficient (α) which quantifies the loss of energy after reflection, and the scattering coefficient (s) which quantifies the diffusion of reflected sound energy (Kuttruff, 2014).

Calculation of room impulse response is based on ray generation starting from the sound source. At the point of ray collision with the interior surface, a secondary source is introduced and secondary rays are emitted from that point. Total reflected sound energy from a wall is a sum of specular and diffuse reflected sound energy. Numerical modelling of specular and diffuse part of reflected energy is described in the literature by introducing the vector modelling (Rindel, 1995). To define the direction of a reflected ray, two vectors are generated, both starting from the collision point. Those are the specular reflection vector and the diffuse reflection vector. The direction of the former one is determined by Snell's law, while that of the latter one is calculated by a random number generator using the probability function according to Lambert's law. Ideal diffuse reflection follows Lambert's law: in any direction (θ, φ) the intensity of the scattered sound is proportional to $\cos(\theta)$, where θ is an angle between direction of reflection and wall normal. Probability function of Lambert's law is $\sin(2\theta)$ (Rindel, 1995). The vector modules are proportional to specular and diffuse sound energy, respectively. Scattering coefficient s is introduced to quantify the proportion of total reflected energy which belongs to diffuse reflection. The module of the diffuse reflection vector is weighted by the scattering coefficient s, and the module of the specular reflection vector is weighted by the factor $(1 - s)$. The direction of the reflected ray is determined by the resulting vector calculated as a vector sum of specular and diffuse reflection vectors (Rindel, 2004). The specular reflection vector and diffuse reflection vector are generated on each wall reflection, but only the resulting vector is further traced. The vector modelling of scattering, described in this way, introduces the probability zone around the specular reflection vector in which the resulting vector is located. Probability in the probability zone is determined numerically.

Simulation programs available on the market contain the modelling of scattering (Christensen, Koutsouris, 2013). In the literature (Savioja, Svensson, 2015) other ways of modelling in room acoustics are described as well. Generally, the scattering appears in three different applications:

1) *Reflection of rays in ray tracing* – Scattering is used for calculation of the ray direction after reflection. Vector-based scattering is applied, and roughness-scattering is combined with edge-scattering. The scattering coefficient value at mid-frequencies is used for the calculation.

2) *Radiation of energy from a secondary source to simulate a late reflection* – Late reflections consist of a dense succession of echoes with diminishing intensity and typically arrive at the listener with a much longer delay after the arrival of the direct component. Late reflections have been linked to a severe degradation of the low-frequency envelope that is essential to speech intelligibility. Reflection-based scattering with the oblique Lambert distribution is applied (Christensen, Rindel, 2005). The calculation is frequency dependent.

3) *Radiation of the scattered part of an early reflection* – "Early reflections" portion of the impulse response is often taken to be the first 100 ms and they are capable of boosting overall speech intelligibility as they can be integrated with the direct sound. Early reflections have a strong influence on spatial impression, i.e., the listener's perception of the listening-space shape. They are used in combination with an image-source calculation of the non-scattered part of reflected energy. The scattered energy is calculated using a large number of secondary sources randomly distributed on the reflecting surface. The Lambert pattern is applied for the directions of the radiation of the secondary sources. The calculation is frequency dependent, which refers to the wave phenomena in the room.

In this paper, a modification of the secondary source modelling in ray tracing simulation is presented, which is used for late reflections (see number 2 from the upper list). The modification introduces an octave band modelling of scattering. The proposed algorithm is tested by comparing the results with measurements in a real sound field obtained in a scaled model.

2. Modification of ray tracing algorithm

In this paper a modification of the secondary source directivity is made by introducing octave band modelling of scattering. The concept of the modification is to change the resulting vector probability zone as a function of the scattering coefficient value. That is based on the statement that the probability zone of the resulting vector is narrow and its axis is oriented in the specular direction when scattering coefficient s is small. Value of the scattering coefficient s is correlated with the probability zone width: by increasing s the zone becomes wider.

The proposed model of diffuse reflection in the ray tracing simulation is illustrated in Fig. 1. Presented

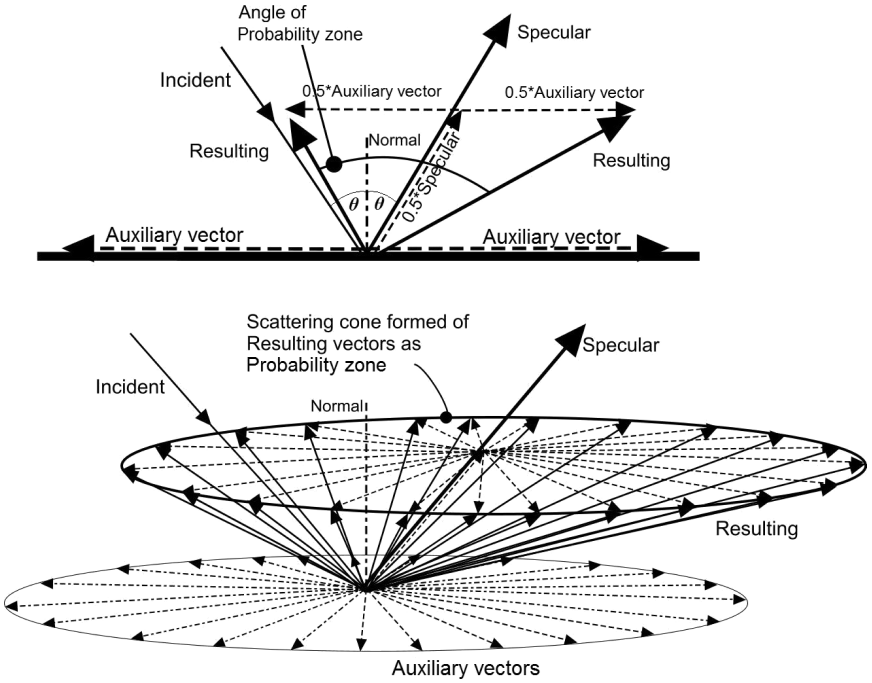

Fig. 1. Illustration of probability zone generation for s = 0.5: top – 2D presentation; bottom – 3D presentation where scattering cone is evident.

are simplified 2D presentation with all related vectors (Fig. 1 top) and 3D presentation where an example of the probability zone is visible (Fig. 1 bottom). In the proposed method the probability zone is created using two kinds of vectors: the auxiliary vectors for creating a scattering cone, i.e. extreme directions of diffuse reflection vector for extremely large s when it is adjacent to the reflection surface (marked in the figure with dashed lines), and the specular reflection vector. Addition of these two vectors, as proposed in vector modelling of scattering, gives the resulting vectors which create a border of the probability zone. This model is arbitrarily constructed in the described way, and is not related to Lambert law, except in the sense of possible diffuse reflections vector's extreme directions, but gives physical interpretation of possible spatial directivity of scattered reflection. In 3D presentation it is visible that the resulting vectors form a cone which is called the "scattering cone", and can be understood as a visual representation of the applied scattering coefficient s.

In Fig. 1 the scattering coefficient $s = 0.5$ is chosen for the reason of drawing simplicity. In that case, for an arbitrary incident angle, specular vector is in the direction determined by Snell's law (incident and reflected angles are the same), and boundaries of the probability zone are determined by resulting vectors (in 2D case, one resulting vector on the left and one resulting vector on the right side). When incident angle to the wall normal increases, direction of the right resulting vector moves closer to the right scattered vector adjacent to the reflection surface, while direction of the left resulting vector moves closer to the wall normal. When the incident angle to the wall normal decreases, direction of the right resulting vector moves to the direction of $\pi/4$ on the right, while direction of the left resulting vector moves to the direction of $\pi/4$ on the left.

Probabilities inside the probability zone, i.e. the scattering cone, are determined in the following way. The scattering cone limits a solid angle in which the resulting diffuse reflection vector can appear, and inside it the secondary source directivity is introduced. To shape this directivity, a solid angle of 2π steradians is divided into equal elements. The solid angle of a spherical segment with arbitrary radius r and arbitrary height h_i, as shown in Fig. 2 (top left), is:

$$\Omega_i = \frac{2r\pi h_i}{r^2} = 2\pi\left(\cos\gamma_{i,1} - \cos\gamma_{i,2}\right), \tag{1}$$

where $\gamma_{i,1}$ and $\gamma_{i,2}$ are angles of the spherical segment's border in the vertical plane. Introducing their difference as $\Delta\gamma_i = \gamma_{i,2} - \gamma_{i,1}$ in the Eq. (1) yields:

$$\Omega_i = 4\pi \sin\left(\frac{\Delta\gamma_i}{2}\right)\sin\left(\gamma_{i,1} + \frac{\Delta\gamma_i}{2}\right). \tag{2}$$

Splitting up the 2π steradians into equal solid angles is shown in Fig. 2 (top). Density of such grid is arbitrary and in this procedure the implemented size of the grid is 10×10 (i.e., 100 equal solid angles). For

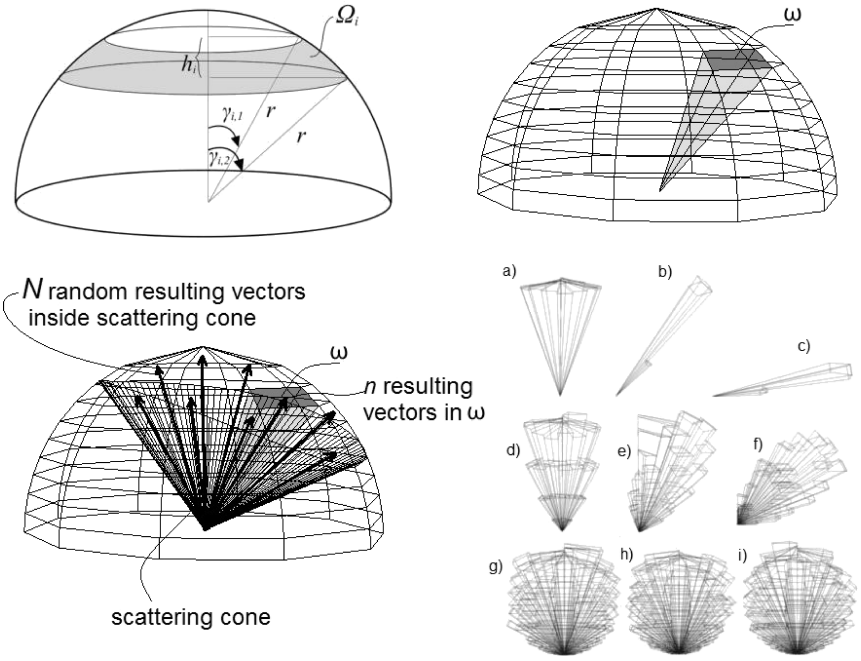

Fig. 2. Top – Illustration of sound intensity calculation inside the scattering cone: top left – solid angle Ω_i of spherical segment with height h_i and radius r; top right – grid 10×10 of equal solid angles ω; bottom left – example of N randomly generated resulting vectors inside the scattering cone; bottom right – examples of directivity diagrams of the secondary source modelled by the scattering cone: $s = 0.1$: a) $\theta = 0°$, b) $\theta = 45°$, c) $\theta = 85°$ (first row); $s = 0.5$: d) $\theta = 0°$, e) $\theta = 45°$, f) $\theta = 85°$ (second row); $s = 0.99$: g) $\theta = 0°$, h) $\theta = 45°$, i) $\theta = 85°$ (third row).

that size of the grid $\Omega_i = 2\pi/10$ [sr], and boundary angles $\gamma_{i,1}$ and $\gamma_{i,2}$ for all 10 spherical segments are determined by recursion. These angles are shown in Table 1, where $\gamma_{i,2} = \gamma_{(i+1),1}$. Equation (2) is solved graphically, and in the first iteration $\gamma_{1,1} = 0$. In the horizontal plane each spherical segment is divided into 10 equal parts ω, and the size of each part is $\omega = 2\pi/100$ [sr]. The grid is shown in Fig. 2 (top, right).

Table 1. Calculated values of boundary angles $\gamma_{i,1}$, $\gamma_{i,2}$ from Eq. (2).

i	1	2	3	4	5	6	7	8	9	10
$\gamma_{i,1}$	0	0.45	0.64	0.79	0.92	1.04	1.15	1.26	1.36	1.46
$\gamma_{i,2}$	0.45	0.64	0.79	0.92	1.04	1.15	1.26	1.36	1.46	$\pi/2$

In the next step of the secondary source directivity shaping, N resulting vectors are randomly generated according to the vector based scattering, as it is shown in Fig. 2 down left. The procedure of sound intensity calculation in each solid angle ω in the grid becomes the counting of resulting vectors inside ω, denoted as n, i.e. n is the number of resulting vectors in the solid angle ω. The final value of the sound intensity in the solid angle ω is the reflected sound power divided by ω:

$$I_\omega = \frac{n}{N}\frac{P_{refl}}{\omega}, \tag{3}$$

where P_{refl} is the reflected sound power of secondary source. Sound intensity in some point at the distance r is calculated as $I_{\omega,r} = I_\omega/r^2$.

By using the described method, a bank of directivity diagrams is made for an array of discrete values of scattering s and incident angle θ. The implemented discretisation of incident angles θ is in the steps of 5° from 5° to 90° and for the scattering coefficient s in the steps of 0.1 from 0.1 to 0.9. The calculated values of directivity are saved in a matrix, as it is shown in Table 2. Sum of all values from Table 2 gives 16.377, which after multiplying with $\omega = 2\pi/100$, gives $1.029 \sim 1$. It means that values in Table 2, after multiplying with $\omega = 2\pi/100$ represent probabilities in the probability zone.

For any given pair (θ, s) the sound intensity in the direction of reflection can be read from the matrix and used in ray tracing calculations. An illustration of directivity diagram for some pair values (θ, s) is shown in Fig. 2 (down right). It can be noticed that for scattering $s = 0.99$ the directivity diagram represents Lambert's pattern and does not depend on the incident angle θ. For that case, quantitative comparison of the directivity diagram with the Lambert's pattern is shown in Table 3.

Table 2. Matrix of I_ω values for grid size 10×10, $s = 0.99$, $\omega = 2\pi/100$, $P_{refl} = 1$, $N = 5000$, acc. to Eq. (3).

φ [rad]	γ [rad]									
	0.157	0.314	0.471	0.628	0.785	0.942	1.099	1.256	1.413	1.570
0.628	0.3257	0.2659	0.1863	0.2397	0.2238	0.1580	0.1302	0.09735	0.03163	0.01816
1.256	0.3024	0.3056	0.2582	0.1707	0.1609	0.1542	0.1065	0.12259	0.06326	0.01090
1.884	0.2171	0.2778	0.2328	0.2143	0.1688	0.1388	0.1302	0.09014	0.03163	0.02906
2.512	0.3179	0.2302	0.2413	0.2506	0.1452	0.1503	0.0908	0.10456	0.04920	0.02543
3.140	0.3606	0.1984	0.1693	0.2034	0.1884	0.1773	0.0789	0.09735	0.05975	0.01453
3.768	0.2869	0.2580	0.2328	0.2070	0.1884	0.1272	0.1342	0.10096	0.03866	0.01453
4.396	0.3024	0.2381	0.2117	0.2360	0.1452	0.1426	0.1579	0.09735	0.04920	0.02543
5.024	0.2869	0.2421	0.1863	0.2215	0.1924	0.1850	0.1144	0.09374	0.04920	0.02180
5.652	0.3722	0.2857	0.3091	0.2288	0.2041	0.1889	0.1460	0.07932	0.04569	0.01816
6.280	0.3373	0.2977	0.2328	0.2469	0.1570	0.1388	0.1381	0.09374	0.03866	0.01090

Table 3. Quantitative comparison of the directivity diagram with the Lambert's pattern for $s = 0.99$.

i	$\gamma = (\pi/2) \cdot i/10$	Lambert's pattern, $\cos(\gamma)$	Directivity diagram, Eq. (3), summed by φ, where γ = const	Difference [%]
1	0.157080	0.987688	1.143634	–15.594500
2	0.314159	0.951057	0.956148	–0.509120
3	0.471239	0.891007	0.831560	5.944681
4	0.628319	0.809017	0.816185	–0.716850
5	0.785398	0.707107	0.652727	5.438018
6	0.942478	0.587785	0.574295	1.348999
7	1.099557	0.453990	0.451559	0.243133
8	1.256637	0.309017	0.359357	–5.034050
9	1.413717	0.156434	0.168035	–1.160010
10	1.570796	6.13E–17	0.069488	–6.948830

Results quality tests have been performed for grid sizes from 10×10 up to 65×65 (see Sec. 5). The sizes below 25×25 have underestimated results in simulation. The size 25×25 meet the expectations regarding the quality of results. The sizes above 25×25 have overestimated results in simulation, and their computation time rapidly increases. An illustration of computation times which depend on the grid size are presented in Table 4. Simulation is calculated for a room of a shoe box shape with dimensions $4 \times 3 \times 2.6$ m, with 1000 rays and 2 seconds time of simulation.

Table 4. Influence of the grid size on time of calculation. Simulation is calculated for a shoe box room $4 \times 3 \times 2.6$ m, with 1000 rays and 2 seconds time of simulation.

Grid size	Time of calculation [s]
10×10	475
14×14	930
18×18	1290
25×25	2230
30×30	3100
65×65	14 080

3. Calculation of impulse response from echogram

Impulse response is a function of sound pressure vs. time. Result of ray tracing simulation is energy vs. time (the echogram). Although there already exist methods of converting the information from energy histogram obtained by ray tracing into an "equivalent impulse response" in literature (Kuttruff, 1993), here we will suggest another method.

As a result of ray tracing, when a ray hits an observation point its sound intensity is registered. All hits, i.e. sound intensities in some time interval $(t,\ t + \Delta t)$, are summed, and as a result an echogram is obtained. Frequency sampling rate is defined as $f_s = 1/\Delta t$. A hit is actually a point in time, and has a broadband frequency response. If instead of a point points which represent Kaiser-Bessel octave band filter in time domain, with f_s sampling rate, are registered, the result will have octave band frequency response.

According to known relation for plane sound waves, sound intensity is proportional to square of sound pressure, $I \sim p^2$. Regarding the fact that Kaiser-Bessel filter in time domain is related to pressure, summing it in this way neglects phase shifts and interference effects between sound waves in the room (Savioja, Svensson, 2015). An alternative suggested here is to try summing in the "intensity domain". For that purpose, each octave band Kaiser-Bessel filter $p_{KB}(t)$ in time domain will be modified according to the following formula:

$$I_{KB}(t) = \text{sign}\left(p_{KB}(t)\right) \cdot p_{KB}^2(t), \tag{4}$$

where $I_{KB}(t)$ is a filter in the "intensity domain", i.e. sound intensity of Kaiser-Bessel filter with the retained sign. As an illustration, Fig. 3 shows signals

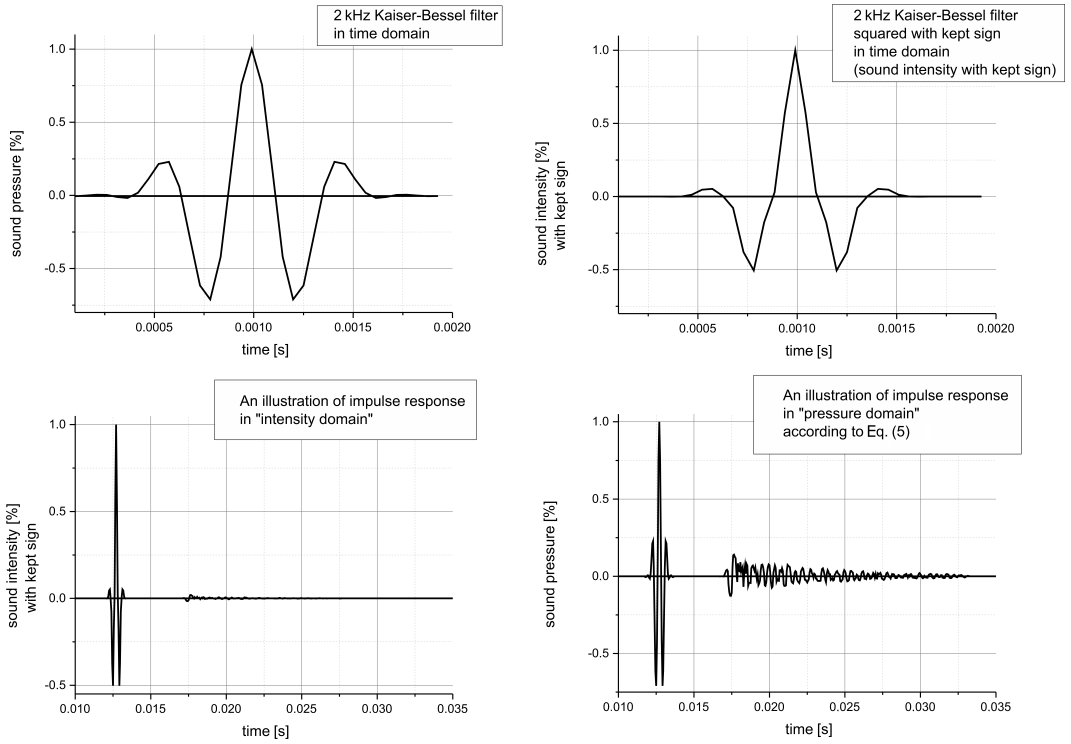

Fig. 3. Kaiser-Bessel filter 2 kHz octave band in time domain $p_{KB}(t)$ (top left). Modified Kaiser-Bessel filter 2 kHz in the "intensity domain" $I_{KB}(t)$, according to Eq. (4) (top right). An illustration of impulse response in the "intensity domain" (bottom left). An illustration of impulse response in the "pressure domain" according to Eq. (5) (bottom right).

$p_{KB}(t)$ and $I_{KB}(t)$ for 2 kHz octave band. Now, after the summing result is the sound intensity with retained sign, Fig. 3 (below left). To get back to the "pressure domain", an inverse operation to Eq. (4) is applied:

$$p_{\Sigma}(t) = \text{sign}\left(I_{\Sigma}(t)\right) \cdot \sqrt{|I_{\Sigma}(t)|}, \tag{5}$$

where $I_{\Sigma}(t)$ is intensity sum in the related band, which represents sound intensity with the retained sign, and $p_{\Sigma}(t)$ represents sound pressure in the related band, Fig. 3 (bottom right). The signal obtained in this way has almost the same magnitude characteristics in the frequency domain as the original Kaiser-Bessel filter. But it is summed in the "intensity domain", which means that the previous remarks regarding phase shifts and interference effects do not hold.

4. Numerical testing of the ray scattering algorithm

The differences between various ray tracing algorithms and the contribution of their potential improvement are hard to quantify on the complex structure of a calculated room impulse response. In order to find a way to improve the algorithm presented in the paper, a computer simulation test is prepared in which the total energy reflected from only one diffusing surface is examined. The idea of such a test is to observe the change of reflected energy from diffusing surface when its scattering coefficient varies.

In the test the diffusing surface is circular. A sketch of model in the test is presented in Fig. 4. The applied diffusing surface radius in the computer simulation is $r = 4.75$ m. In the computer simulation the value of absorption coefficient $\alpha = 0.1$ is assigned to the diffusing surface for all frequencies. The sound source and the observation point are positioned at a distance $d = 4$ m and at such a height from the surface so that the incident angle and the angle of specular reflection are 45°, as it is shown in Fig. 4. The source and the observation point are positioned so that the point of specular reflection is in the centre of the circular diffusing surface. The impulse response consists of the direct sound and reflected energy from the entire diffusing surface. Octave band dependent values of s used for computer simulation of a diffuse reflection are presented in Table 5.

Table 5. Scattering of the surface from Fig. 4 by octave bands (Vorlander, Mommertz, 2000).

f [Hz]	63	125	250	500	1000	2000	4000	8000
Scattering	0.01	0.05	0.2	0.45	0.55	0.7	0.75	0.8

The results of simulation are shown in Fig. 5. Only characteristic 4 octave bands are shown, but impulse responses from all 8 octave bands are calculated. In simulations Kaiser-Bessel octave band filters in 37 points have been used (Collins, 2017). The illustrations in Fig. 5 show that an increase of scattering coefficient prolongs the impulse response in time, despite the fact that the size of the diffusing surface remains constant. In reality, the average impulse response value (mean value of sound pressure) is 0. To come closer to reality, impulse responses from Fig. 5 should be convolved with the filtered direct sound recorded in an

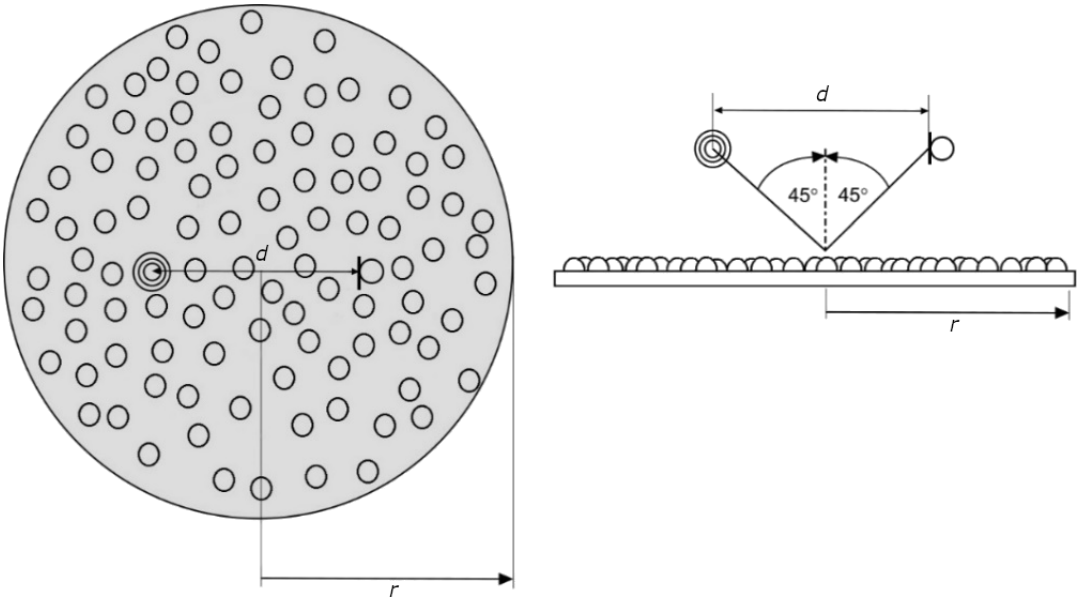

Fig. 4. Diffusing surface used for numerical and experimental tests. For the numerical tests $r = 4.75$ m, scattering coefficient s from Table 4 was used. For the experimental tests the 1:10 scale model was used with $r = 47.5$ cm, the disc was 50% covered with 4 cm wooden calottes.

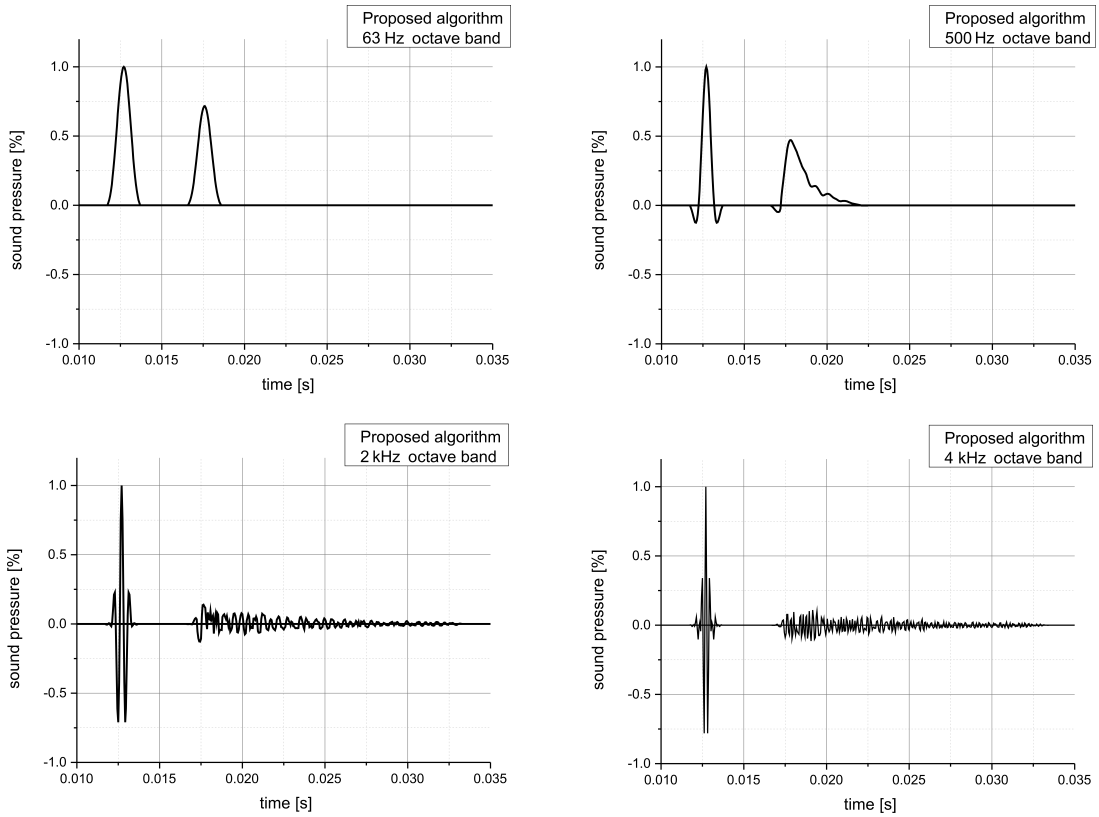

Fig. 5. Illustration of impulse response simulation with proposed algorithm for diffusing surface in Fig. 4, through characteristic octave bands with scattering values from Table 4.

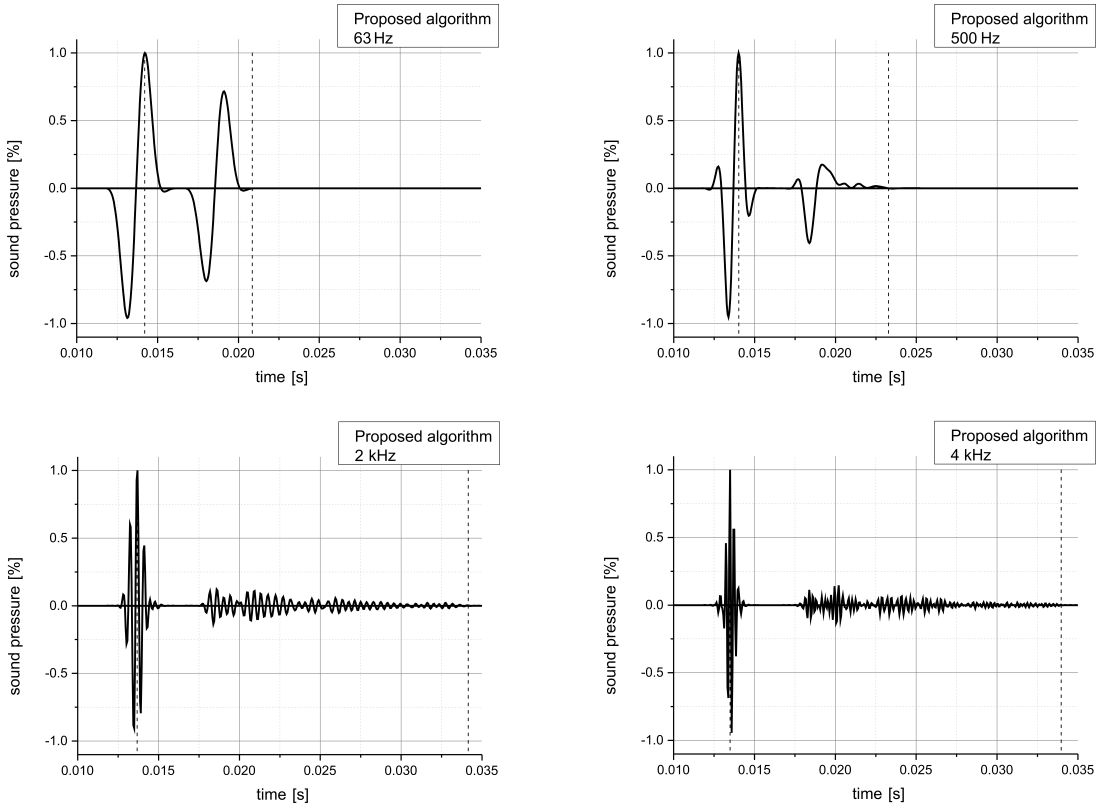

Fig. 6. Impulse responses from Fig. 5 after convolution with filtered direct sound recorded in the experiment shown in Fig. 7 resampled to 19.2 kHz, through octave bands. Dashed lines: impulse response length.

experiment shown in Fig. 7 resampled to 19.2 kHz. Filtering is done with the same Kaiser-Bessel octave band filters in 37 points. Convolution is done according to the following C++ procedure:

```
double * proc_convolution(double *signal, int
num_signal, double *filter, int num_filter)
{
   double sum = 0;
   double * convolution = new double[num_sig-
   nal + num_filter - 1];
   for (int i=0; i<(num_signal + num_filter -
   1); i++)
   {
       for (int j=0; j<num_filter; j++)
       {
          if (((i - j) >= 0) && ((i - j) <
          num_signal))
          {
          sum = sum + filter[j]*signal[i - j];
          }
       }
     convolution[i] = sum;
     sum = 0;
   }
   return convolution;
}
```

where *convolution* is the result, *num_signal* is the number of samples in the impulse response denoted as *signal*, *filter* is Kaiser-Bessel octave band filter, length of Kaiser-Bessel filter is *num_filter*.

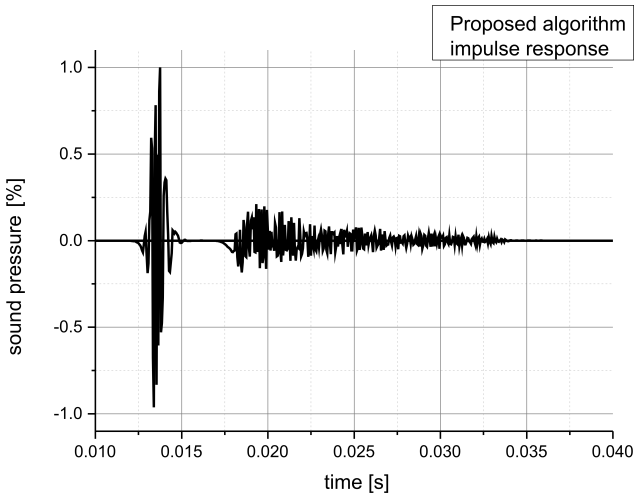

Fig. 7. Impulse response obtained by the proposed algorithm.

The results after convolution are shown in Fig. 6. The impulse response length in time related to its direct sound, through octave bands is presented in Table 6 (impulse response length interval is denoted in Fig. 6 by dashed lines).

The process of creating a unified wideband impulse response using octave band impulse responses is described here. First, impulse responses from Fig. 6 (including all octave bands, not only those shown) are converted into the "intensity domain" as it is it described in Sec. 3. Impulse responses shouldn't be normalised to maximum pressure amplitude of 1. The second step is to sum all impulse responses in the "intensity domain", and convert the obtained impulse response into the "pressure domain". The impulse response obtained in this way is shown in Fig. 7.

5. Experimental testing of the ray scattering algorithm

To verify the modelling results two methods have been used. The first one is measuring impulse response in a physical model. The second one is a simulation with a commercial software.

For the first method, 1:10 physical model has been used (Fig. 4). The diffusing structure consists of 4cm hemispheres (wooden calottes), stochastically distributed and covering about 50% of the laminated surface. That concept is symbolically presented in Fig. 4. Radius of the spheres is chosen to be 4 cm due to the fact that the results of scattering coefficient measurement can be found in literature for such type of relief (Vorlander, Mommertz, 2000). In the experiment, an electrical spark generator (Šumarac-Pavlović *et al.*, 2015), and standard 1/4″ measuring microphone have been used. Signal acquisition is performed with the sampling frequency 192 kHz and with 24 bits resolution. All impulse responses are normalised to maximum pressure amplitude of 1.

The result of the experiment in the form of impulse response of reflected energy at the receiver position is presented in Fig. 8. The results of its filtering by Kaiser-Bessel octave band filters are shown in Fig. 9. Regarding the fact that sampling is done

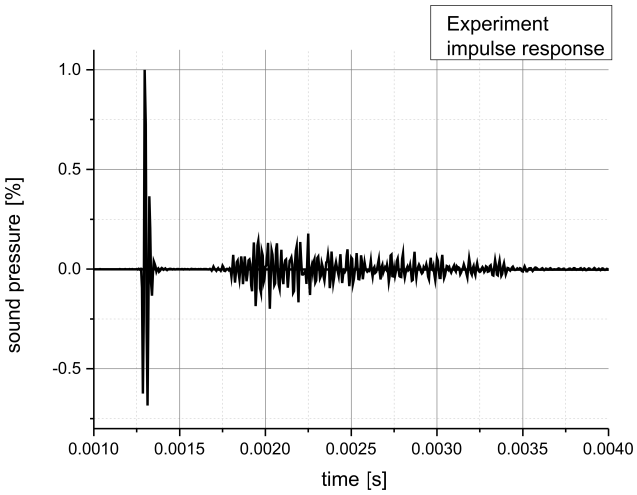

Fig. 8. Impulse response recorded in the experiment.

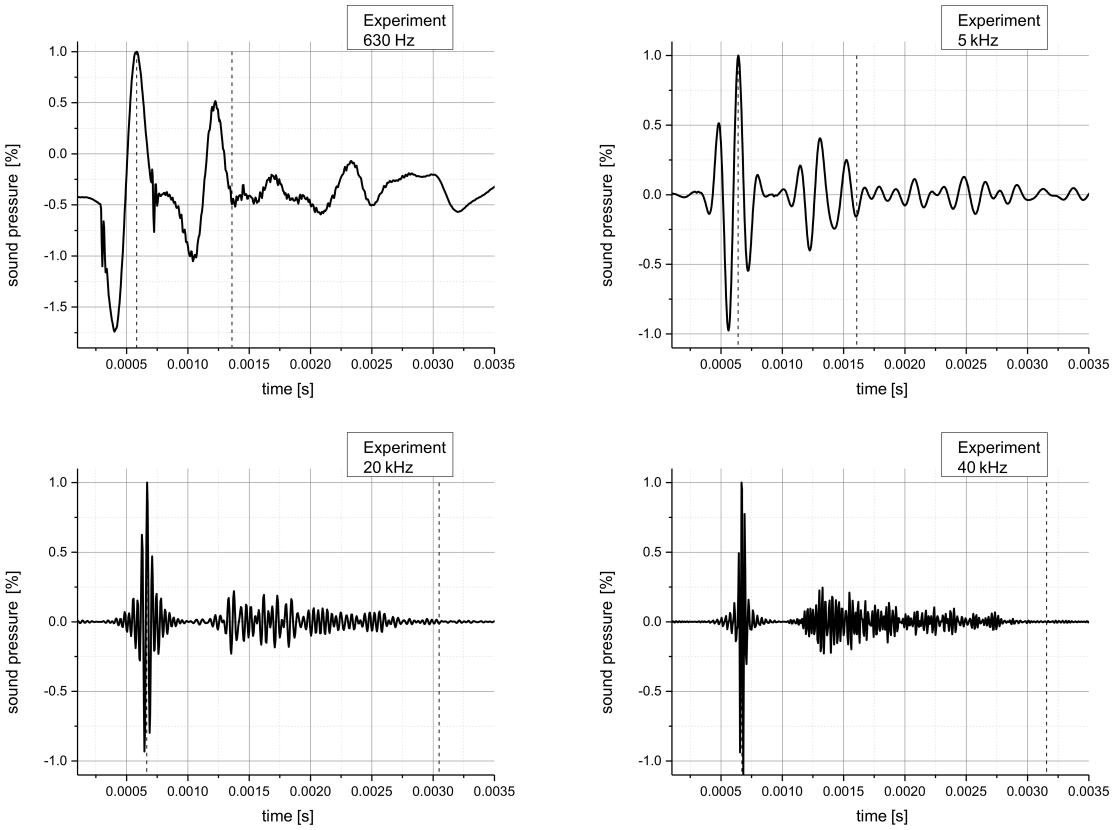

Fig. 9. Impulse response recorded in the experiment filtered by Kaiser-Bessel octave band filters, whose central frequencies are multiplied 10 times as compared to those in the simulation. Dashed lines: impulse response length.

with frequency 192 kHz, central frequencies of octave band filters are multiplied 10 times (630 Hz, 1250 Hz, 2500 Hz, 5 kHz, 10 kHz, 20 kHz, 40 kHz, 80 kHz). The number of points of Kaiser-Bessel filter should be chosen as (79, 79, 99, 119, 139, 139, 139, 139) respectively, to get clear results. The time axis of the impulse responses recorded in the scale model should be multiplied 10 times to compare them with the simulation results.

For the second method, a simulation with a commercial piece of software is used. The same surface model is used for simulation as it is described previously in Sec. 4. The result of simulation is presented in Fig. 10. The results of its filtering by Kaiser-Bessel octave band filters are shown in Fig. 11.

The impulse response lengths obtained from the experiment, proposed algorithm and simulation with the commercial software are presented in Table 6.

To provide numerical comparison of the calculation, experiment, and simulation with the commercial software, parameters from ISO 3382 standard are used (ISO 3382-1, 2009). Obtaining decay curves by reverse-time integration of the squared impulse responses from Fig. 7, Fig. 8, and Fig. 10 enables calculation of the reverberation time. The reverberation time can be evaluated based on a smaller dynamic range than 60 dB and extrapolated to a decay time of 60 dB. In Fig. 12 sound decay curves based on the reverberation tail of impulse responses from Fig. 7, Fig. 8, and Fig. 10, normalised to start from (0, 0) for easier comparison, are shown. The time axis for the experiment is multiplied by 10, due to the 1:10 physical model.

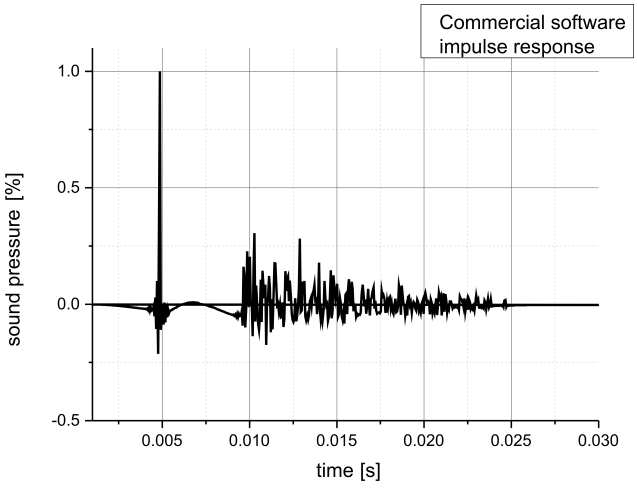

Fig. 10. Impulse response simulated with a commercial software.

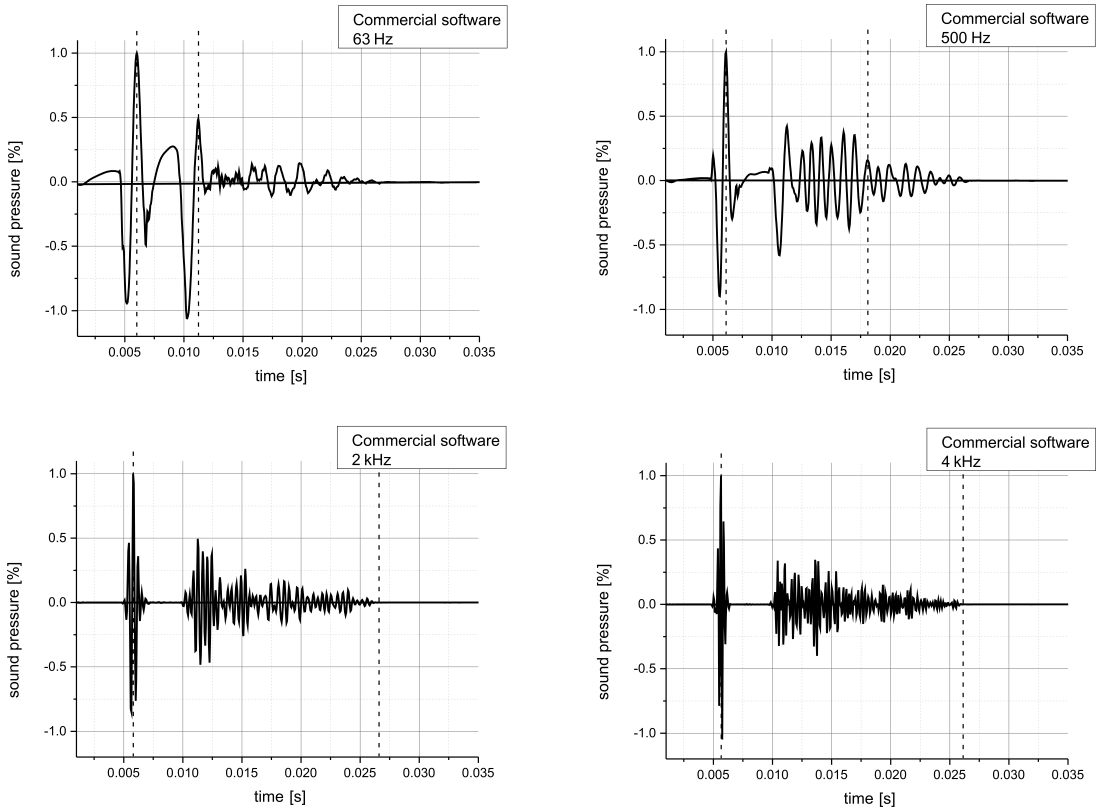

Fig. 11. Impulse response simulated with a commercial software, filtered by Kaiser-Bessel octave band filters. Dashed lines: impulse response length.

Table 6. Impulse response lengths from Fig. 6, Fig. 9, and Fig. 11 by octave bands.

f [Hz]	630	5k	20k	40k
Impulse response length from experiment [ms] × 10	7.71	9.50	23.7	23.9
Impulse response length from proposed algorithm [ms]	6.70	9.30	20.7	20.8
Difference proposed algorithm from experiment [%]	13.00	0.02	12.6	12.9
Impulse response length from commercial software [ms]	5.10	11.20	20.1	20.0
Difference commercial software from experiment [%]	33.00	–17.80	15.0	16.0

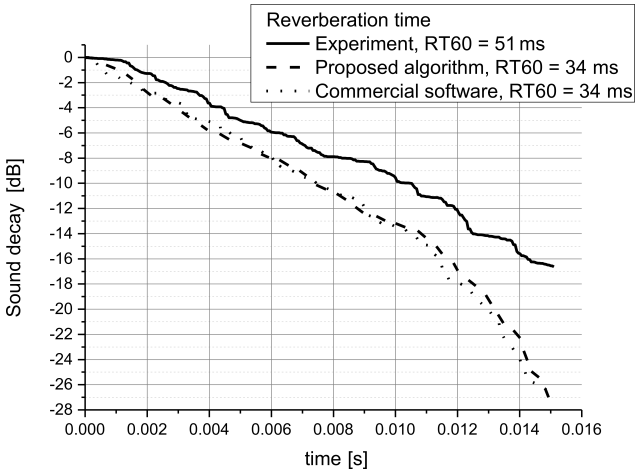

Fig. 12. Comparison of decay curves and reverberation times for impulse responses from the experiment, proposed algorithm, and commercial software.

6. Conclusion

The paper suggests an innovative model for the octave band modelling of scattering in room acoustics computer modelling. In the paper a modification of the ray tracing algorithm based on change in modelling secondary sources in diffuse reflections is shown. This modification aims at enabling reliable impulse response simulation of partial models of a room (Šumarac-Pavlović, Mijić, 2010), where the goal is not the whole impulse response but contribution of certain surfaces. The compatibility of proposed modelling, experimental results and simulation with the help of a commercial software is confirmed by comparing the impulse response lengths and reverberation times.

References

1. Christensen C.L., Rindel J.H. (2005), *A new scattering method that combines roughness and diffraction effects*, Forum Acousticum, Budapest.
2. Christensen C.L., Koutsouris G. (2013), *Odeon Room Acoustics Software*, User Manual, Ver. 12, 2nd Ed., Ch. 6.3.
3. Collins A.R. (2017), *FIR Filter Design*, Miscellaneous Technical Articles, from https://www.arc.id.au/FilterDesign.html.
4. ISO 3382-1 (2009), *Measurement of room acoustic parameters*, reference number ISO 3382-1:2009(E).
5. Krokstad A., Strom S., Sorsdal S. (1968), *Calculating the acoustical room response by the use of a ray tracing technique*, Journal of Sound and Vibration, **8**, 1, 118–125.
6. Kuttruff H. (2014), *Room acoustics*, 5th Ed., Spon Press, Milton Park.
7. Kuttruff H. (1993), *Auralization of impulse responses modeled on the basis of ray-tracing results*, Journal of the Audio Engineering Society, **41**, 11, 876–880.
8. Rindel J.H. (1995), *Computer simulation techniques for acoustical design of rooms*, Acoustics Australia, **23**, 81–86.
9. Rindel J.H. (2004), *Odeon and the scattering coefficient*, Pdf-formatted Power Point Presentation from Odeon Workshop at Baltic-Nordic Acoustical meeting, Mariehamn.
10. Savioja L., Svensson U.P. (2015), *Overview of geometrical room acoustic modeling techniques*, Journal of the Acoustical Society of America, **138**, 2, 708–730.
11. Šumarac-Pavlović D., Mijić M. (2010), *Partial scale models as a tool in acoustic design*, 1st EAA–EuroRegio, Ljubljana.
12. Šumarac-Pavlović D., Mijić M., Mašović D. (2015), *The influence of proscenium boxes on acoustic response in historical opera halls*, Journal of Acoustical Society of America,**138**, 2, 420–425.
13. Vorländer M. (2013), *Computer simulations in room acoustics. Concepts and uncertainties*, Journal of the Acoustical Society of America, **133**, 3, 1203–1213.
14. Vorlander M., Mommertz E. (2000), *Definition and measurement of random-incidence scattering coefficients*, Applied Acoustics, **60**, 2, 187–199.